Available online at www.sciencedirect.com
ScienceDirect
Magnetic Resonance Imaging 29 (2011) 739–751
MAGNETIC RESONANCE IMAGING

Original contributions

DTI at 7 and 3 T: systematic comparison of SNR and its influence on quantitative metrics

Seongjin Choi[a], Dustin T. Cunningham[a], Francisco Aguila[a], John D. Corrigan[b], Jennifer Bogner[b], W. Jerry Mysiw[b], Michael V. Knopp[a], Petra Schmalbrock[a,*]

[a]Department of Radiology, The Ohio State University, Columbus, OH 43210, USA
[b]Department of Physical Medicine and Rehabilitation, The Ohio State University, Columbus, OH 43210, USA

Received 24 August 2010; revised 29 December 2010; accepted 20 February 2011

Abstract

Diffusion tensor imaging (DTI) and advanced related methods such as diffusion spectrum and kurtosis imaging are limited by low signal-to-noise ratio (SNR) at conventional field strengths. DTI at 7 T can provide increased SNR; however, B0 and B1 inhomogeneity and shorter T2∗ still pose formidable challenges. The purpose of this study was to quantify and compare SNR at 7 and 3 T for different parallel imaging reduction factors, R, and TE, and to evaluate SNRs influences on fractional anisotropy (FA) and apparent diffusion coefficient (ADC). We found that $R>4$ at 7 T and $R\geq 2$ at 3 T were needed to reduce geometric distortions due to B0 inhomogeneity. For these R at 7 T, SNR was 70–90 for b=0 s/mm^2 and 22–28 for b=1000s/mm^2 in central brain regions. SNR was lower at 3 T (40 for b=0 s/mm^2 and 15 for b=1000 s/mm^2) and in lateral brain regions at 7 T due to B1 inhomogeneity. FA and ADC did not change with MRI field strength, SENSE factor or TE in the tested range. However, the coefficient of variation for FA increased for SNR <15 and for SNR <10 in ADC, consistent with published theoretical studies. Our study demonstrates that 7 T is advantageous for DTI and lays the groundwork for further development. Foremost, future work should further address challenges with B0 and B1 inhomogeneity to take full advantage for the increased SNR at 7 T.

Keywords: DTI; 7 T; SNR; Partial volume effects

1. Introduction

Quantitative diffusion tensor imaging (DTI) has found many clinical applications including traumatic brain injury (TBI) [1–4], multiple sclerosis [5], brain tumors [6] and stroke [7]. White matter structure can be assessed by DTI metrics such as fractional anisotropy (FA) and apparent diffusion coefficient (ADC) allowing for better understanding of the brain's structural networks in health and disease.

Though DTI is very promising, challenges exist because there is still much variability in reported DTI metrics. For example, reported FA values for the genu range from 0.50 to 0.82 for control subjects and 0.50–0.84 in TBI patients [1–3]. Reasons for variability in DTI metrics include differences in acquisition and analysis approaches. Specifically, FA differences have been associated with different field strengths [8–11] and diffusion gradient schemes [12,13]. DTI metrics are also profoundly affected by partial volume effects [14–17] and are thus related to voxel size and shape. Further, FA was found to increase with decreasing signal-to-noise ratio (SNR), whereas mean diffusivity decreases with increasing SNR [18]. Computer simulation studies have shown that variability in DTI metrics become especially pronounced for very low SNR [18–22].

Magnetic resonance imaging (MRI) at ultra-high field strength (e.g., 7 T) increases SNR, but shorter T2∗ and T2, increased static field (B0) and radiofrequency (RF) field (B1) inhomogeneity may offset the SNR advantage. B0 inhomogeneity will lead to increased image distortion and shorter T2∗ introduces blurring and signal loss with long echo trains in echo-planar imaging (EPI). B1 inhomogeneity will cause local signal losses due to decreased flip angles. Additional artifacts may be introduced because fat suppression may be compromised due to B0 and B1 inhomogeneity. Finally, motion and physiologic noise artifacts may become more prevalent with 7 T.

* Corresponding author.
E-mail address: schmalbrock.1@osu.edu (P. Schmalbrock).

0730-725X/$ – see front matter © 2011 Elsevier Inc. All rights reserved.
doi:10.1016/j.mri.2011.02.009

The higher SNR at 7 T may be translated into (1) smaller voxels thus reducing partial volume artifacts, (2) more *b*-directions in reasonable scan times by avoiding the need for signal averaging and/or (3) larger *b*-values needed, e.g., for diffusion spectrum imaging (DSI) [23] and diffusion kurtosis imaging (DKI) [24]. In optimizing acquisition protocols, a careful balance has to be achieved between spatial and diffusion directional resolution, SNR in high *b*-value diffusion weighted images, and minimizing artifacts.

The primary objective of this study was to characterize and quantify SNR in the acquired diffusion weighted images and its influence on DTI metrics, FA and ADC, at 7 T and 3 T as a function of parallel imaging reduction factor *R* and echo time (TE), as it is clear from preliminary studies [25,26] and studies comparing 1.5T and 3 T DTI [8,10,11,27,28] that parallel imaging is needed to reduce distortion. A secondary aim was to evaluate how the achievable SNR, and other factors, including voxel size and shape, partial volume effects and analysis approach, affect FA and ADC measurements.

To date, 7 T DTI has been limited to feasibility and exploratory studies [8,9,26,29–32]. To the best of our knowledge, quantitative assessment of the potential advantages of 7 T DTI compared to standard field strengths has not yet been published. Availability of this information will allow devising strategies for optimizing acquisition approaches for 7 T DTI.

2. Methods

2.1. Acquisition

Eleven healthy subjects with ages ranging from 24–56 years (six males/five females) were studied. Institutional review board-approved consent was obtained. Images were acquired at 7 T (Philips, Achieva, Cleveland, Ohio) using a 16-channel receive coil with a head volume transmit coil (Nova, Medical); 3 T data were acquired using an 8 channel receive coil and the body transmit coil (Philips, Achieva, Best, Netherlands). The maximum gradient strength was 33 mT/m at 7 T and 80 mT/m at 3 T. Diffusion weighted images were acquired using a single shot spin echo echo-planar sequence (SE-EPI). One b=0 s/mm^2 and 6 or 15 b=1000 s/mm^2 diffusion-weighted images were acquired using the Philips "overplus" mode which allows for shortest TE. K-space coverage was 80%. Fat suppression was done with spectral presaturation inversion recovery (SPIR) [33]. At 7 T, TR=5800–10500 ms was longer than at 3 T where TR=3200–4500 ms due to specific absorption rate restrictions leading to scan times of about 9 min per DTI acquisition. In addition, at 7 T, high-resolution susceptibility weighted images were acquired using a 3D gradient echo sequence with TR/TE/Flip angle=24.5 ms/12 ms/5° and 0.4×0.5×1.6 mm^3 voxel size, and B1 maps were acquired using scanner tools [34]. At 3 T, additional anatomic T1 and/or T2 weighted images were acquired.

In the first phase of the study, a range of SNR values was achieved by varying the parallel imaging Sensitivity Encoding (SENSE)-factor (R=2–7), TE and by taking measurements in brain regions that have different flip angles in order to evaluate the impact of SNR on DTI metrics. 7 T and 3 T DTI data were acquired on one subject (24 years) with 2-mm isotropic voxels (reconstructed on the scanner to 1.5×1.5×2 mm^3), 15 gradient directions with b=1000 s/mm^2 and no signal averaging. To determine SNR with SENSE reconstruction, it was necessary to acquire two data sets, one with the RF on and a second with RF off for noise determination. Using scanner tools, we also reconstructed g-factor maps from the coil sensitivity calibration scans [27,35]. Sets of scans with minimum TE for all R-factors (TE_R=57–75 ms at 7 T, and TE_R=53–59 ms at 3 T), and with fixed TE=75 ms for all R-factors were acquired.

In the second phase of the study, we evaluated partial volume effects from different acquisition protocols and analysis approaches on DTI metrics. Ten subjects (31–56 years) were imaged at 7 T using R=5 and at 3 T using R=2. Five different spatial and diffusion directional resolution protocols were tested including 2×2×2 mm^3 and 1.6×1.6×3.2 mm^3 with six and 15 directions, and 2.0×2.6×5 mm^3 with six directions. Data were minimally interpolated by 10–30% in the in-plane direction using rounding limitations imposed by the scanner software. All these data used three averages for the b=1000 s/mm^2 images and TE=56–75 ms.

2.2. Analysis

All images were visually examined for distortion and artifacts. Distortion was semi-quantitatively assessed following the approach by Alexander et al [14], i.e., lines were drawn on images with different R-factors to evaluate the distortion (Fig. 1).

For SNR analysis in the first phase of the study, the RF on/off images were evaluated using custom IDL tools (ITT Visual Information Solutions, Boulder, CO, USA) and DtiStudio [36]. Small regions of interest (ROIs) (11–32 pixels) were manually drawn on the axial images for the body, genu and splenium of the corpus callosum (CC), for the posterior limb of the internal capsule (PLIC) and in a subcortical white matter region (SCWM). SNR was determined as signal in the RF "on" images divided by the standard deviation of noise in the RF "off" images. Median filtering was explored but not used for the final analysis. Experimentally measured SNR was compared to the expected behavior of SNR decrease with R-factor [27] (Fig. 2, Table 1).

For motion and eddy current correction, all diffusion weighted images were registered either with the registration tools available in the scanner (Philips FiberTrak) or with the registration methods in DtiStudio (mutual information based registration). For analysis of large central fibers, choice of registration methods did not produce noticeable differences.

For the analysis of the first phase of the study, FA and ADC values were obtained on axial imagines in the same

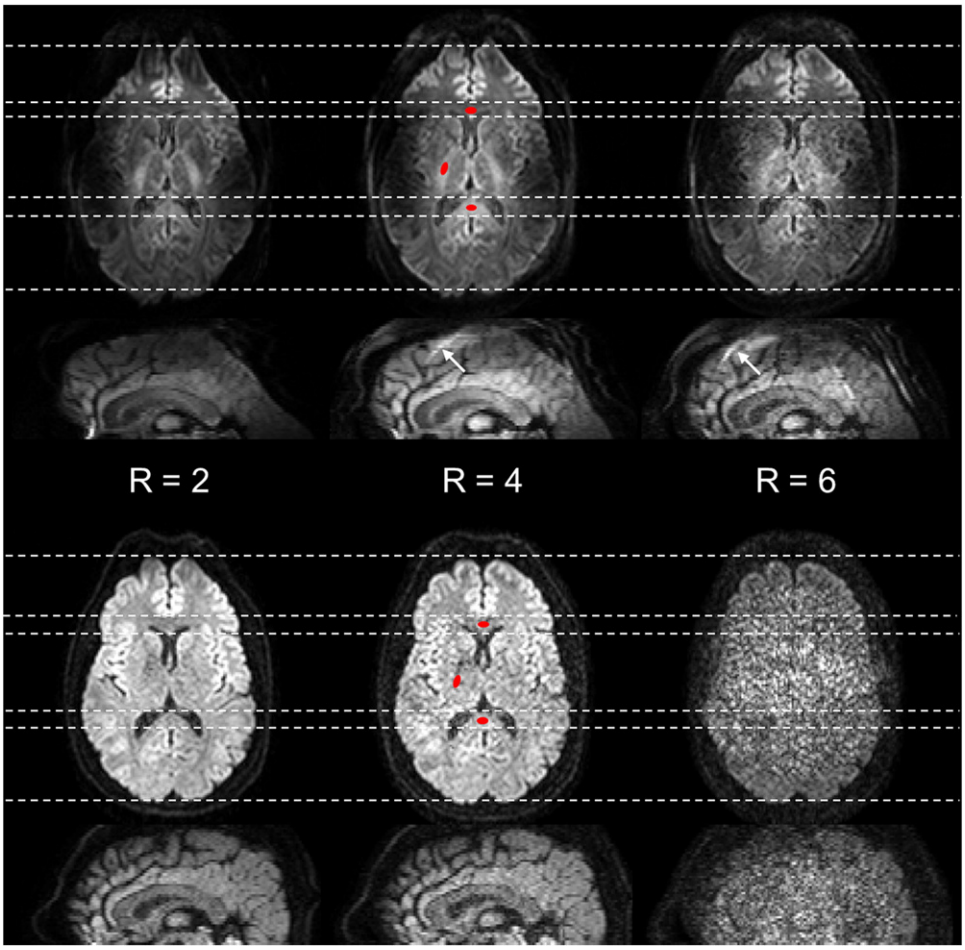

Fig. 1. Example average axial and reformatted sagittal b=1000 s/mm^2 diffusion-weighted images at 7 T (top) and 3 T (bottom). Comparison of data from R=2, 4 and 6 demonstrate the excessive distortion for low R-factors at 7 T (see dashed lines). Distortions are reduced for R=6 at 7 T albeit at the expense of lower SNR. For 3 T, distortions are still visible for R=2. Also note the signal decrease in the lateral and superior-anterior parts of the brain at 7 T due to B1 inhomogeneity, which also leads to imperfect fat suppression and ghosting of fat signal (white arrows). The observed contrast between 7 T and 3 T, b=1000 s/mm^2 images is different due to residual T2 effects. In the basal ganglia, T2 for the caudate and putamen with high iron content are relatively shorter at 7 T than at 3 T. Adjacent white matter appears brighter likely due to a combination of these T2 effects and the higher B1 in the central part of the brain. Red ROIs show the regions used for analysis in the genu (GCC), splenium (SCC) and PLIC.

ROIs used for the SNR analysis without further interpolation of the data beyond the initial interpolation by the scanner software (Figs. 3–5). Mean FA and ADC, standard deviations σ_{FA} and σ_{ADC} and coefficients of variation $CV_{FA}=100*\sigma_{FA}/FA$ and $CV_{ADC}=100*\sigma_{ADC}/ADC$ were computed from voxel-based spatial ROI statistics.

For the second phase of the study, various analysis approaches were explored on selected examples. Initially, FA and ADC maps were analyzed using MRI scanner tools. Color-coded FA maps from axially acquired images were reformatted to a mid sagittal plane showing the CC as a well-defined red structure. The entire CC and regions including the genu (GCC), body (BCC) and splenium (SCC) were manually traced along the red area. This approach lead to inclusion of a significant number of voxels beyond the boundary of the CC and resulted in severe partial volume effects. To avoid boundary voxels, the red CC was traced narrowly such that all included voxels stayed within the visible CC (Fig. 6). To make the analysis observer and software independent, the initial testing also included a repeated analysis of FA and ADC maps in DtiStudio. The corpus callosum was selected automatically on a mid-sagittal section, by setting thresholds for FA of 0.35, 0.47 and 0.70. Each threshold setting effectively selected a ROI in the CC that was contaminated with partial volume effects, completely contained within the CC, or comparable to the small manually placed ROIs.

Finally, the entire data set of the second phase of the study (i.e., the data on 10 subjects with five different acquisition protocols at both field strengths) was analyzed as follows: first, small ROIs in the genu were manually traced on sagittally reformatted images (a) along the red boundary of the genu, (b) excluding the edge voxel and (c) including only the most central voxels of the genu. Second, the entire corpus callosum visible in red on sagittal reformatted color coded FA maps was manually traced. Third, the traced ROI of the

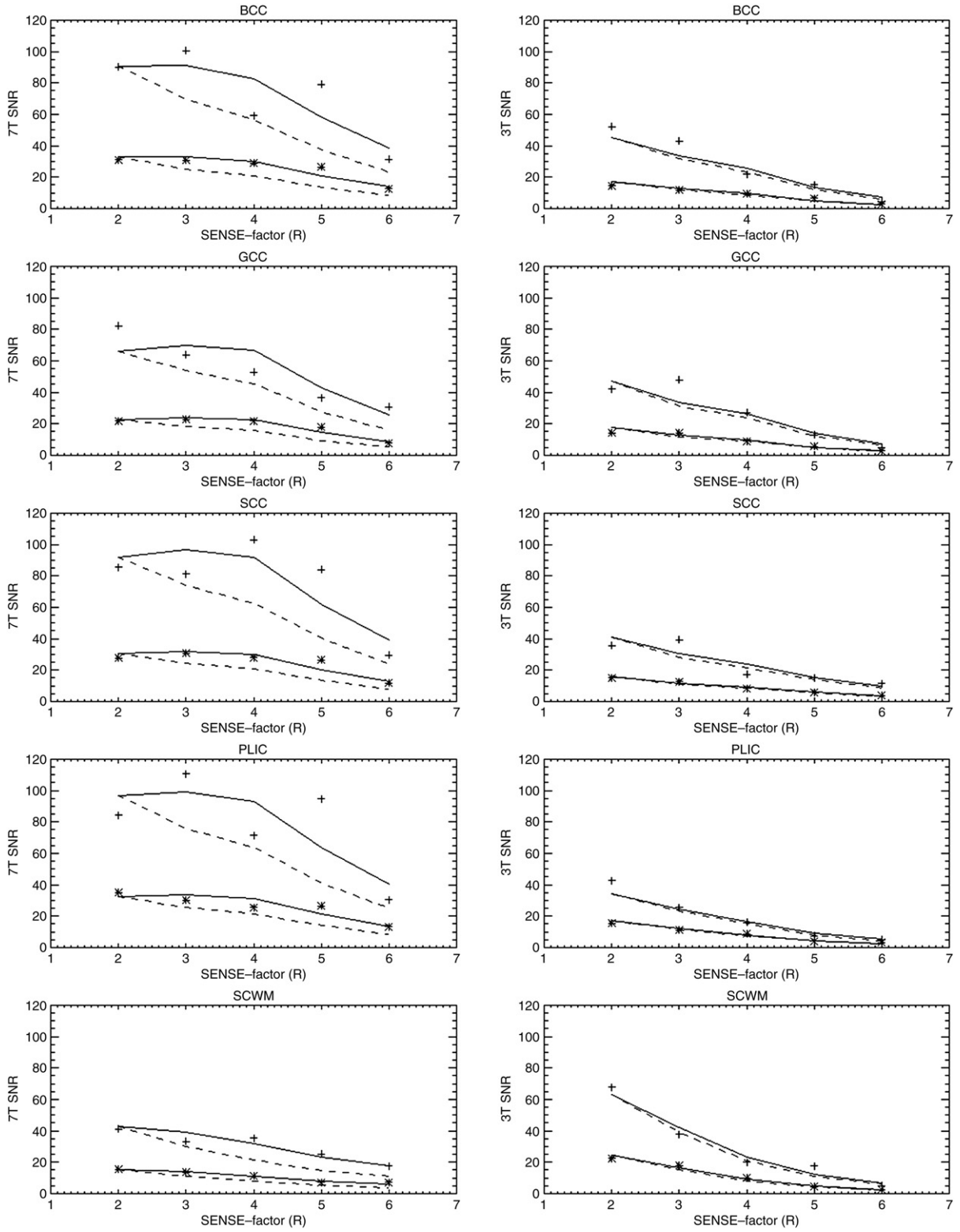

Fig. 2. SNR as a function of SENSE-factor R for 7 T (left) and 3 T (right). Example data are shown for the BCC, GCC and SCC the PLIC and a frontal SCWM. Shown are measured SNR values for b=0 s/mm^2 (+) and b=1000 s/mm$_2$ (∗) and using shortest TE. The solid lines represent fits according to Eq. (1) for minimal TE and dashed lines represent SRN estimates for the longer fixed TE for all R-values. For central brain regions, SNR at 7 T is 2.5–3-fold larger than at 3 T (see text and Table 1). This advantage is lost for lateral brain due to B1 inhomogeneity.

Table 1
Example SNR for b=1000 s/mm^2 in different brain regions R-factors and field strength

ROI	7 T				3 T	
	Flip angle	Fit SNR_{full}	Exp R=4	Exp R=5	Fit SNR_{full}	Exp R=2
BCC	81	408	28.2	26.4	90	14.2
GCC	65	279	22.8	18.8	94	14.1
SCC	78	367	27.9	26.5	82	15.0
PLIC	61	394	25.7	26.6	89	15.5
SCWM	39	198	11.2	7.2	140	22.5

entire red CC was used for single-ROI streamline tractography using Philips FiberTrak. Mean FA and ADC and standard deviations, i.e., voxel-based ROI statistics for all traced ROIs were recorded. Likewise, means and standard deviations for all voxels contained in the streamlines were recorded without interpolation of the data. We refer to the mean FA and ADC data from the entire tract as tract-of interest (TOI) value [37].

2.3. Statistics

Repeat measurements of the same subject at different field strengths were analyzed using paired t test. The data from the second phase of the study with different spatial and directional resolution were evaluated (1) by simply computing mean values and standard deviations for each acquisition and analysis method over all 10 subjects and (2) with analysis of covariance (ANCOVA) using age as a covariate, to provide multi-subject group statistics. ANCOVA was used to remove the age effect on the DTI metrics from the subject pool, which had a large age range.

3. Results

3.1. Image quality assessment

Fig. 1 demonstrates distortion and SNR for different SENSE-factors R. At 7 T, very severe distortion artifacts are seen in the frontal brain regions for R<4. Distortion improves with increasing R, which reduces the echo train length. Distortion is not visible in the right/left direction or in the central part of the brain such that the selected ROIs (BCC, GCC, SCC and PLIC) are not affected. Severe distortions are also seen on reconstructed sagittal sections. The 3-T images of the same volunteer show some distortion for the R=2 images but distortions are largely avoided for larger R. On the other hand, SNR visibly decreases with increasing R. The loss of SNR becomes particularly noticeable for R>5 in the 7 T/16-channel coil data and becomes prohibitively low for R>2 in the 3 T/eight-channel coil images.

The 7 T images also show significant effects for B1 inhomogeneity with lower flip angles leading to signal loss in lateral regions of the brain (Fig. 1). The flip angle map shows a 2-3-fold decrease in the lateral regions compared to the central parts of the brain for the RF transmit coil used in this study (Table 1). Since the signal for the SE-EPI sequence follows the $S \propto \sin^3(\alpha)$ relationship, this local reduction in flip angle leads to a 4-10 fold signal loss in lateral brain regions. Consequently, 7 T performs visibly better for R=3–5 than 3 T with R=2 in the central parts of the brain, but this advantage is reduced or lost in lateral brain regions with the current RF transmit technology.

Suppression of fat signal from the skull is less favorable at 7 T than at 3 T (Fig. 1). This difference is due to B1 inhomogeneity since the SPIR fat suppression technique relies on well performing inversion pulses and B0 homogeneity for successful suppression of fat. Especially with large R-factors, some banding/ghost artifacts can occur. Since the banding is identical for all b-values/directions these ghosts propagate into DTI metrics maps. They can be recognized and avoided for ROI analysis but may contaminate tractography.

3.2. SNR measurements

Fig. 2 shows the measured SNR as a function of the SENSE factor, R, and shortest achievable TE_R for different white matter regions (Fig. 1) in a representative subject. The experimental data follow the expected relationship, below, and indicated by the solid lines in Fig. 2.

$$\mathrm{SNR}(R) = \frac{\mathrm{SNR}_{full} exp(-TE_R / T2)}{g_R \sqrt{R}} \quad (1)$$

The factor g_R was measured for the selected brain regions from g-factor maps that were generated from the coil sensitivity profiles by scanner manufacturer provided software. SNR_{full} is the average scaling factor for fitting the experimental data with the theoretical curve (Table 1). The relaxation time factor $\exp(-TE_R/T2)$ was estimated from a previous study using dual echo spin echo T2 measurements [38]. Values of T2=35 ms for 7 T and T2=45 ms for 3 T were used for the line-plots in Fig. 2. For illustrative purposes, the plots of the 7 T data in Fig. 2 also include the expected SNR for fixed TE=75 ms for all R. It can be seen that, for R=3–5, the SNR loss with can be recovered by the shorter achievable TE_R. For R=6 and 7, this is no longer the case, largely because the g-factor becomes much larger than one, resulting in severe SNR reduction.

SNR decreases about two- to threefold between the b=0 s/mm^2 and b=1000 s/mm^2 images and this is consistent with ADC values of 0.75–0.9 ($\times 10^{-3}$mm^2/s) in white matter regions. As DTI metrics are influenced by SNR from the image data in all b-directions, it is also important to assess SNR differences in the different b-directions. For the 7-T R>5 data with average SNR of 22–28 (Table 1), measured SNR values for individual directions range from a minimum of 10–14 to a maximum of 35–40. For 7 T data with R=6, this range decreases to 3.5–14, and for R=7 to 1.5–7, which

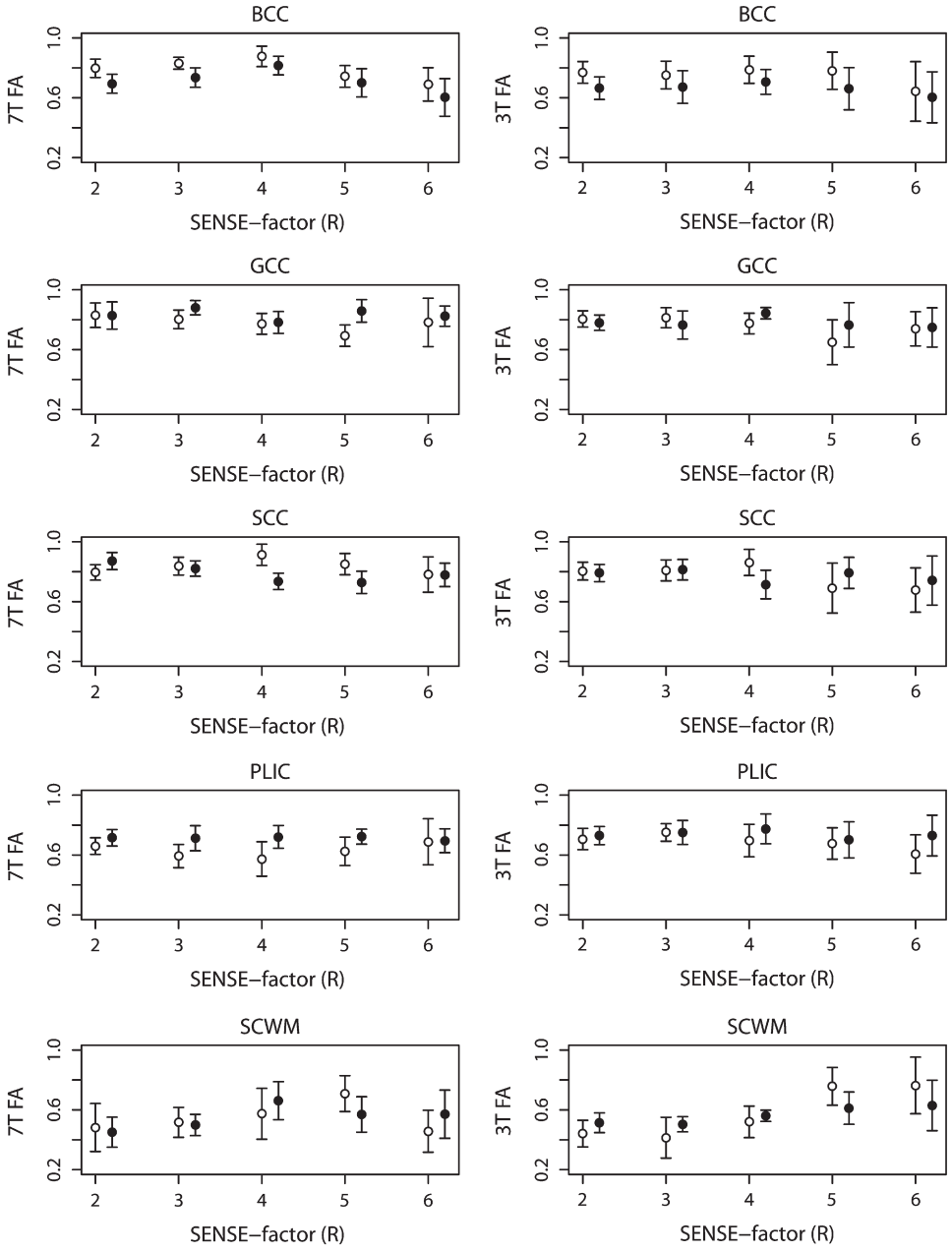

Fig. 3. Voxel-based mean FA as a function of SENSE factor *R* for 7 T (left) and 3 T (right) for the BCC, GCC, SCC, PLIC and SCWM. Solid symbols represent the measurements for shortest achievable TE, open symbols are data for longer, fixed TE. All data were measured for integer values for *R*, but are offset for plotting purposes. Note that the standard deviation error bars increase with increasing *R* due to lower SNR especially at 3 T.

will introduce errors in subsequent DTI metrics. For 3 T with R=2, the average SNR=15, ranging from 7 to 20 in different gradient directions in the b=1000 s/mm^2 images.

3.3. FA and ADC-value and their Coefficients of Variation depending on SNR (R, TE)

Fig. 3 shows FA values for the small ROIs selected on axial images (Fig. 1) for the body, genu and splenium of the corpus callosum (BCC,GCC, SCC), the PLIC and for a SCWM. FA values for the body and splenium of the corpus callosum (BCC, SCC) are similar to the GCC. With few exceptions, overall FA as a function of R value showed similar values. FA values from the minimal TE data are not drastically different from the fixed TE data. Further, FA shows similar values at both field strengths (7 T and 3 T). FA variability in terms of standard deviation gradually increases accordingly with increasing R values. For the selected small ROI (11–32 voxels), values in different regions of the corpus callosum and PLIC are similar; FA is apparently smaller in peripheral SCWM regions.

ADC values for the GCC, BCC, SCC, PLIC and SCWM are similar except for data with SNR<10 in the high b-value

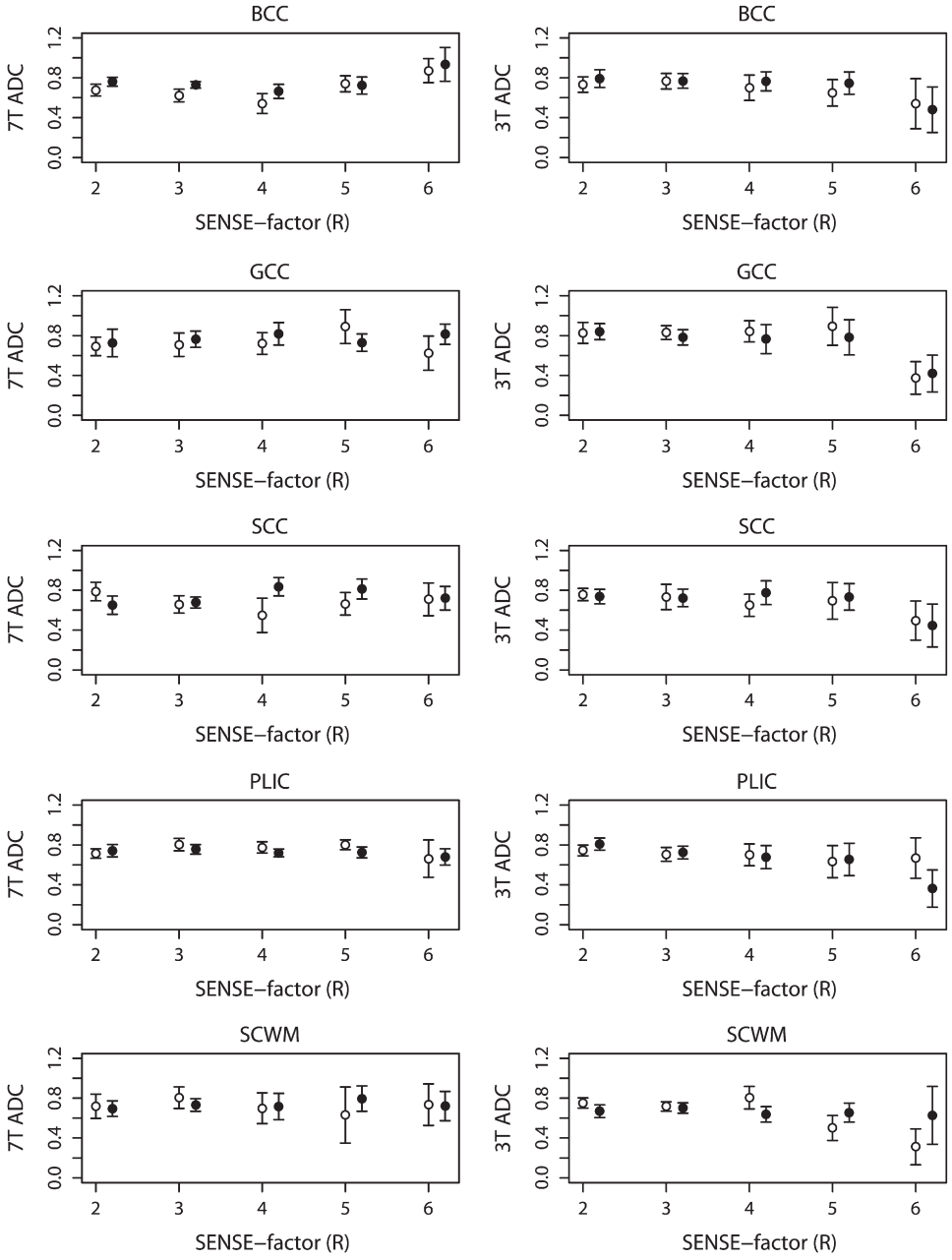

Fig. 4. Voxel-based mean ADC as a function of SENSE- factor *R* for 7 T (left) and 3 T (right) for the BCC, GCC, SCC, PLIC and SCWM. Solid symbols represent the measurements for shortest achievable TE, open symbols are data for longer, fixed TE. All data were measured for integer values for *R*, but are offset for plotting purposes. Note that the standard deviation error bars increase with increasing *R* due to lower SNR especially at 3 T.

diffusion images (Fig. 4). Similar ADC values are observed in most ROIs that were selected. There is no drastic difference between the fixed and minimum TE data or between field strengths. As observed in overall trends in variability of FA, standard deviation of ADC gradually increases with increasing *R* values.

While mean FA and ADC values do not change notably with *R*, TE or field strength, significant increase in the standard deviations of FA and ADC values are observed for the noisier large *R*/long TE data (error bars in Figs. 3 and 4). This is also much more noticeable in the 3 T data. Fig. 5 shows the mean, standard deviation and CV for FA and ADC as a function of average SNR in the b=1000 s/mm^2 images. For the analyzed small ROIs that were selected sufficiently far away from grey matter (GM) or cerebrospinal fluid (CSF) spaces to avoid partial volume effects, FA and ADC measurements vary by about 10% as long as SNR>15. Once SNR becomes smaller than 10, a fairly sharp increase in the CV of FA is observed (Fig. 5, left bottom). Likewise, an increase in CV for ADC is observed for SNR<10 (Fig. 5 right bottom). Note that the average SNR <10 in the b=1000 s/mm^2 diffusion-weighted images corresponds to SNR <3–5

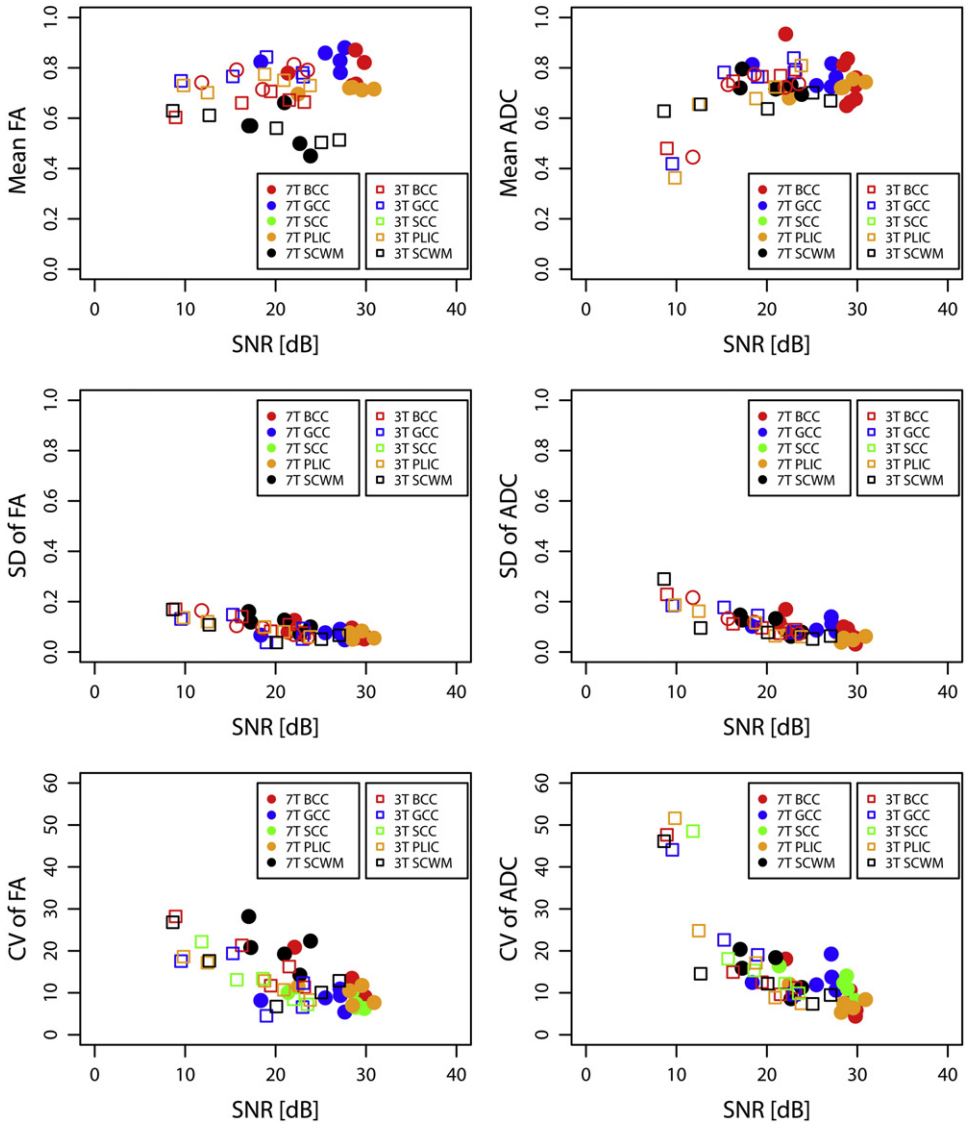

Fig. 5. Mean (top), standard deviation (middle) and CV (bottom) for FA (left) and ADC (right) as a function of SNR in dB using SNR[dB]=20log$_{10}$(SNR) [19] for the minimum TE data. Solid symbols represent 7 T data, open symbols are for 3 T. Different brain regions are in different colors (red-BCC, blue-GCC, green-SCC, orange-PLIC, black-SCWM). Note the increase in the CV for FA for SNR <15 (23 dB) and for ADC for SNR <10 (20 dB) in the b=1000s/mm^2 images.

for some gradient directions, and this will significantly affect all DTI metrics.

3.4. Demonstration of partial volume effects in the slice direction

An example case for the evaluation of partial volume effects in the data at different resolutions is shown in Fig. 6. The top row shows an overlay of sagittally reformatted color coded FA maps for three different axial slice thicknesses on high-resolution susceptibility-weighted images. For the 2 mm slice thickness, FA maps showing the red boundary of the corpus callosum correspond well to the anatomic outline seen on the susceptibility-weighted images. With increasing slice thickness the boundary of the CC on the FA map gets "washed out." Tracing the visible boundary of the red CC on non-interpolated color FA maps leads to inclusion of boundary voxels outside the CC especially for thicker slices (Fig. 6, turquoise ROIs). As a result, mean FA values are lower and have large standard deviations (voxel based ROI statistics: 0.70±0.23, 0.59±0.24 and 0.50±0.19 for 2-, 3.2- and 5-mm slice thickness respectively; turquoise bars in Fig. 6, bottom left). Restricting the tracing to a narrow strip in the center of the CC (Fig. 6, orange ROI) increased FA and decreased the standard deviations (voxel based ROI statistics: 0.70±0.17, 0.71±0.17 and 0.56±0.19 for 2-, 3.2- and 5-mm; orange bars in Fig. 6, bottom left). Selection of small ROIs on sagittal images comparable in size to the ROIs selected for the SNR, FA and ADC analysis listed in Figs. 3 and 4 gave similar mean FA and CV (voxel-based ROI statistics: 0.82±0.10, 0.81±0.09 and 0.70±0.16, black bars in Fig. 6 bottom left) except for the very thick slices. Analogous

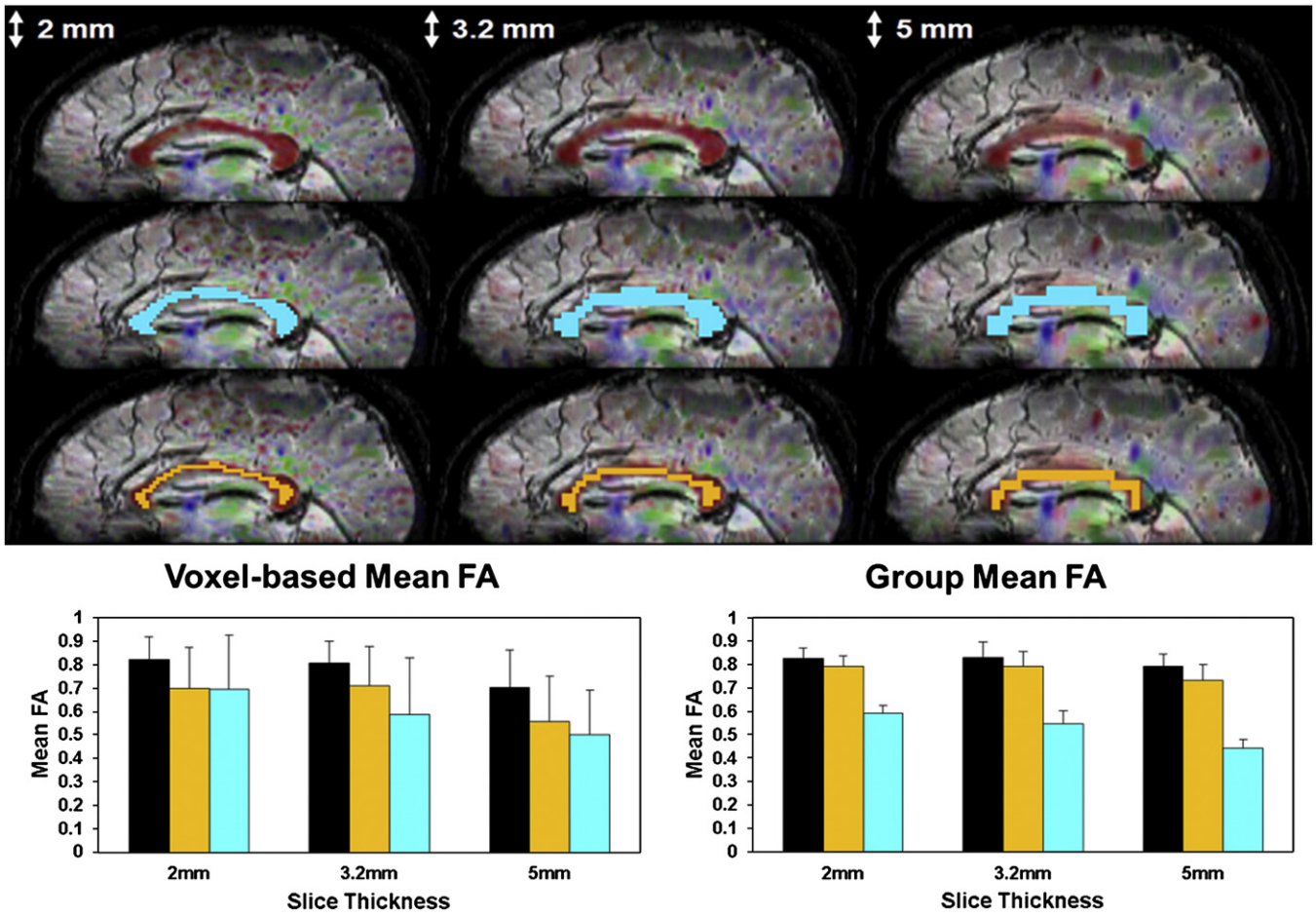

Fig. 6. Sample partial volume effects with increasing slice thickness. Sagittally reformatted color FA maps are overlaid on high resolution susceptibility weighted images (top row). For 2-mm slice thickness, there is a good match between the FA map and the anatomical image. FA maps are progressively washed out for increasing slice thickness. Voxel-based ROI statistics bottom left: ROIs defined by manually tracing the red boundary on the FA maps (turquoise ROIs) will lead to inclusion of voxels extending beyond the CC resulting in decreased mean FA values with large standard deviations (turquoise bars). Selecting a narrower trace (orange ROI) excludes boundary voxels and increases FA (orange bars). Selecting very small ROIs in the GCC or SCC (analogous to the analysis used in Figs. 3 and 4) further increases mean FA and decreases its standard deviation (black bars). Note that FA values are lower for thicker slices. Group average of all 10 subjects (bottom right) for the GCC for 2-, 3.2- and 5-mm slice thickness (wide trace along the red boundary: turquoise bar, excluding boundary voxels: orange bar and including only central voxels: black bars).

results were obtained with changing the selected FA threshold in DtiStudio for ROI selection.

3.5. Protocol comparison study

Group mean FA values for all 10 subjects for three different manual tracing methods of the genu are shown in the bottom right part of Fig. 6. The same pattern observed for single subject voxel-based ROI statistics is maintained in the group averages of all 10 subjects, i.e., the widest tracing along the red boundary yields lowest group mean FA (0.59, 0.55 and 0.44 for 2, 3.2- and 5-mm slice thickness; turquoise bar Fig. 6, bottom right); narrower tracing increases group mean FA (0.79, 0.79 and 0.73; orange bars), and largest group mean FA is observed for small central ROIs (0.83, 0.83 and 0.79, black bars Fig. 6, bottom right). Similar observations were made for ADC measurements not shown. The observation that group mean averages of multiple subjects show the same pattern as voxel-based ROI statistics may indicate that quantitative DTI metrics are consistent as long as consistent methods are used.

Table 2 shows the group mean FA values calculated with ANCOVA using age as a covariate for the data from all 10 volunteers. Group mean ROI values were computed from the entire corpus callosum seen in red on reformatted mid-sagittal sections. Group mean TOI values were computed from each subject's tract averaged FA values including all voxels in the tract through the CC using Philips FiberTrak. As in the wide ROI analysis (Fig. 6 bottom right, turquoise bars), group mean FA values for the entire cohort of subjects are lower than the small ROI data shown in Fig. 3 and the narrow tracing in Fig. 6 (bottom right, black bar). In all cases, values for thinner slices are higher than for thicker slices, i.e., group mean $FA_{2\ mm} > FA_{3.2mm} > FA_{5\ mm}$. This is statistically significant ($P<.01$) for all pair-wise comparisons. Group mean FA values for the 15 gradient direction

Table 2
Partial volume effects and ROI vs. TOI analysis

Acquisition method	ROI		TOI	
	7 T	3 T	7 T	3 T
2×2×2, 15 dir	0.558	0.568	0.600	0.598
1.6×1.6×3.2, 15 dir	0.509	0.509	0.569	0.576
2×2×2, 6 dir	0.578	0.600	0.625	0.632
1.6×1.6×3.2, 6 dir	0.508	0.544	0.600	0.599
2×2.6×5, 6 dir	0.427	0.424	0.518	0.493

data tend to be lower than the six direction data; however, this difference was not statistically significant in most cases. ROI data are lower than TOI data ($P<.05$). There is no statistically significant difference between 7 T and 3 T FA measurements ($P>.05$).

4. Discussion

Our study shows that for the tested conditions, FA and ADC do not significantly change with B0 field strength or TE as long as SNR is sufficiently high (Figs. 3, 4). Assessment of the CV for small regions of interest well contained within a specified white matter structure (Fig. 5) indicated that average SNR for b=1000 s/mm^2 should be larger than 10, corresponding to SNR (b=0 s/mm^2) >30. For these SNR limits, SNR drops below 3 for some gradient directions in the high b-value diffusion weighted images and affects DTI metrics. By example, we also showed that partial volume effects especially between WM and CSF/GM but also within different WM fiber structures will have the most pronounced effect on numerical values and variability of DTI metrics (Fig. 6). Nevertheless, consistent results can be achieved as long as the same acquisition parameters and a consistent analysis approach are used (Table 2).

4.1. B0 and TE effects

Our finding that FA and ADC do not change with B0 field strength is consistent with one study comparing 1.5 T and 3 T [28] but different from a preliminary report by Polders et al [8] who showed an FA increase with field strength from 1.5 to 7 T. Increase in FA with field strength was also reported in 3 T/1.5 T comparison studies by Huisman at al [11] and Qin at al [10]. These latter two studies concluded that the observed differences in FA may be attributed to SNR and TE differences rather than to field strength. This conclusion is consistent with our finding that for very small ROIs, FA/ADC differences are predominantly due to SNR. In our study, TE ranged from 57–75 ms for 7 T and 53–59 ms (75 ms used for fixed TE) for 3 T. With T2=35 ms at 7 T and T2=45 ms at 3 T [38], these TE lead to significant signal loss, especially at 7 T (7 T: exp(−TE/T2)=0.12 to 0.20; 3 T: exp(−TE/T2)=0.19 to 0.31). However, no significant variability was observed for FA and ADC as TE was changed with R-factor because, for the longer TE, the R-factor was smaller and SNR remained sufficiently high. The observed variability in FA and ADC seems to be explained when SNR reaches critically low values (<10 in diffusion weighted images). To further assess if there is a change with TE, a future study would have to be done with a fixed R-factor and a wider range of TE.

4.2. SNR

Our finding that, for small ROI, SNR significantly influences FA and ADC is consistent with prior experimental findings. For example, Alexander et al. [28] reported decreasing FA with increasing SNR. Similar to our study, Polders et al. [9] reported increased variability in FA measurements with decreasing SNR.

The reported experimental findings are consistent with computer simulations. Pierpaoli et al. [39] showed that, for low SNR, the longitudinal principal Eigenvector λ1 was overestimated, whereas the Eigenvectors λ2 /λ3 are underestimated, leading to overestimation of FA for low SNR. Jones [12] and Kristofferson [20] showed that for SNR <3, the signal bias due to the Rician rather than Gaussian signal distribution cannot be neglected and needs to be included in computation of diffusion tensors. Koay et al [21,22] showed that for SNR <5 tensor estimation methods may become unstable and lead to deviations in DTI metrics. Landman et al. [18] developed a theoretical framework to model the influence of noise in DTI and showed how it affects different tensor estimation methods and acquisition protocols. They showed (Fig. 2 in Ref. [18]) that for SNR <40 db in b=0 s/mm^2 images, mean FA and standard deviation of FA increase. ADC was less affected than FA, but decreases in ADC and increased standard deviation for ADC were pronounced for SNR <25 dB in b=0 s/mm^2 images (Fig. 2 in [18]). Using SNR[dB]=20log$_{10}$(SNR) [19], and assuming a factor 2–2.5 for the SNR decrease between b=0 s/mm^2 and b=1000 s/mm^2 images, our measurements for the CV for FA and ADC as a function of SNR (Fig. 5) are comparable to the theoretical simulations by Landman et al. [18]. In our study, standard deviations for both FA and ADC increased with decreasing SNR. As in Landman's study, mean ADC decreased with decreasing SNR; the net effect is the sharp rise in CV for ADC with small SNR (Fig. 5). Mean FA values were more variable but, overall, tended to be flat with SNR. The relation of FA with SNR may be somewhat biased in our study because low SNR values were realized predominantly by large R-factors and lower field strength (Fig. 5) but also by low regional flip angles in SCWM where FA may be lower due to less compact and or crossing fibers.

Consistent with prior experimental and theoretical simulations studies, our studies showed that accurate DTI metrics require average SNR>10 for b=1000 s/mm^2 diffusion weighted images. This corresponds to SNR>25 (about 30 dB) in the T2-weighted b=0 s/mm^2 images but will lead to SNR of about 3 in the high-b-value diffusion-

weighted images for some gradient directions. As already pointed out by Landman [18,19], a significant amount of 3-T DTI research is below this SNR limit. Consequently, many studies employ signal averaging even though theoretical studies proclaim the benefit of acquiring more *b*-directions rather than more signal averages, likely because most simulations assumed higher SNR [13].

4.3. Partial volume effects

Our exploratory analysis (Fig. 6) indicated that the largest differences in numerical values for FA and ADC are due to partial volume effects. Though not comprehensive, our analysis is analogous to the erosion/dilation method used by Pfefferbaum [15] and shows similar findings. Similar results were also reported in a recent simulation study [16]. It has been shown that partial volume issues may be addressed by using a multicompartment approach for the diffusion tensor fitting [14,40–42]; however, partial volume limitations are, in general, better addressed by higher spatial resolution.

Despite the differences in numerical values for FA and ADC, our findings demonstrated that consistent results are achieved as long as identical acquisition and analysis methods are used. Table 2 shows that values for FA are numerically different for different spatial and directional resolution, and for the TOI and ROI analysis. Nevertheless, data obtained for each specific approach are consistent. We also previously showed [43] that linear regression of FA and ADC values with the subjects' age resulted in identical slopes (i.e., statistically nonsignificant differences in slope) but different intercepts ($P<.05$) for the data acquired with different spatial and directional resolution. This consistency observed for fixed acquisition and analysis methods is encouraging for clinical DTI studies comparing patient with control groups.

4.4. Advantages of 7 T

The findings described here suggest that it is of paramount importance to decrease voxel sizes while maintaining adequate SNR levels. DTI at higher field strength is uniquely suited to accomplish this, but acquisition methods have to be optimized. For example, given the experimental conditions in our 7 T study (16-channel receive coil, R=4–5 for minimizing distortion), we estimate an average SNR ≈11–14 in the b=1000 s/mm^2 diffusion-weighted images for 1.5×1.5×1.5 mm^3 voxels and SNR ≈5–10 for 1×1×1 mm^3 voxels. Thus, for the conditions tested in our study, 1.5-mm isotropic resolution is feasible without the need for signal averaging, whereas smaller voxel sizes will require further SNR improvements because SNR will drop below 3 for some diffusion directions. Similarly, one may estimate the SNR drop with higher *b*-values. Our measured SNR=22–28 for b=1000 s/mm^2 and 2-mm isotropic voxels (Table 1) would decrease to SNR ≈8–10 for b=2000 s/mm^2 and to SNR ≈2–3 for b=3000 s/mm^2 when assuming a diffusion coefficient of 0.8 and considering the TE increase required for larger b. Thus, b=2000 s/mm^2 and 2-mm isotropic voxels are feasible at 7 T, but larger *b*-values will require larger voxels or other methods of increasing SNR.

4.5. Future improvements

The preceding discussion shows that 7 T can help improve DTI. However, improvements are needed to take full advantage of the increased SNR at 7 T. Foremost, B1 inhomogeneity needs to be improved, or else, the SNR advantage over 3 T is lost for regions with low B1. Multichannel transmit technology [44] is under development commercially and/or utilization of traveling wave excitation may prove a suitable alternative [45]. Better B1 homogeneity will also improve fat suppression and, thus, reduce residual ghosting of fat signal with parallel imaging [46]. Alternatively, fat suppression methods that are more robust to B0 and B1 inhomogeneity could be implemented. Second, distortions due to B0 inhomogeneity still pose a problem, even though distortions could be significantly reduced with high *R*-factors. Further improvement can be achieved with a larger number of receiver array coils and/or multi-shot EPI methods such as readout-segmented EPI [32,47]. Though reduction of distortions from B0 inhomogeneity is preferably done as part of the acquisition process, advanced post-processing methods may further reduce the problem [48]. Another alternative would be reduced field-of-view DTI [30,49,50]. Finally, as discussed above, it is desirable to further improve SNR. At 7 T, the long TE required for high *b*-values with standard body gradient coils (33–40 mT/m) are a major factor reducing available SNR by a factor of 5–10. Head gradient coils were proposed to reduce the duration of the diffusion gradients and TE. This approach may be most favorable in very high b-value methods such as DSI and DKI. For DTI requiring b≈1000 s/mm^2, significant SNR improvement is available with stimulated echo acquisition mode (STEAM) DTI without the need for head gradients. Though STEAM has factor two SNR disadvantage compared to SE sequences, the 5–10-fold SNR loss with long TE is avoided [30,38] because magnetization is stored in the longitudinal direction and thus magnetization decays with T1 which is longer at 7 T. While our study used only six and 15 diffusion directions, more directions can be used at 7 T, e.g., whole-brain DTI using 60 diffusion encoding directions with 1.5-mm isotropic voxels at 7 T can be achieved in approximately 10 minutes.

While 7-T DTI holds great promise, significant future refinements will be needed in order to optimize the advantage of higher SNR achievable at ultra-high field strengths.

Acknowledgment

This work was supported by The Wright Center of Innovation in Biomedical Imaging at The Ohio State

University, Ohio Department of Development (AGMT TECH 03-051).

References

[1] Inglese M, Makani S, Johnson G, Cohen BA, Silver JA, Gonen O, et al. Diffuse axonal injury in mild traumatic brain injury: a diffusion tensor imaging study. J Neurosurg 2005;103:298–303.

[2] Kraus MF, Susmaras T, Caughlin BP, Walker CJ, Sweeney JA, Little DM. White matter integrity and cognition in chronic traumatic brain injury: a diffusion tensor imaging study. Brain 2007;130:2508–19.

[3] Lipton ML, Gellella E, Lo C, Gold T, Ardekani BA, Shifteh K, et al. Multifocal white matter ultrastructural abnormalities in mild traumatic brain injury with cognitive disability: a voxel-wise analysis of diffusion tensor imaging. J Neurotrauma 2008;25:1335–42.

[4] Niogi SN, Mukherjee P, Ghajar J, Johnson CE, Kolster RA, Sarkar R, et al. Extent of microstructural white matter injury in postconcussive syndrome correlates with impaired cognitive reaction time: a 3T diffusion tensor imaging study of mild traumatic brain injury. Am J Neuroradiol 2008;29:967–73.

[5] Kezele IB, Arnold DL, Collins DL. Atrophy in white matter fiber tracts in multiple sclerosis not dependent on tract length or local white matter lesions. Mult Scler 2008;14:779–85.

[6] Cruz LCH, Sorensen AG. Diffusion tensor magnetic resonance imaging of brain tumors. Magn Reson Imaging Clin N Am 2006;14: 183–202.

[7] Mukherjee P. Diffusion tensor imaging and fiber tractography in acute stroke. Neuroimaging Clin N Am 2005;15:655–65.

[8] Polders D, Hoogduin H, Donahue MJ, Henrikse J, Luijten P. Comparison of SNR and diffusion parameters on 1.5, 3.0 and 7.0 Tesla. Proceedings of the Seventeenth Annual Meeting of the International Society of Magnetic Resonance in Medicine. Honolulu; 2009. p. 1406.

[9] Polders DL, Leemans A, Hoogduin JM, Hendrikse J, Donahue M, Luijten PR. Evaluating the uncertainty of DTI parameters at 1.5, 3.0 and 7.0 Tesla. Proceedings of the Eighteenth Annual Meeting of the International Society of Magnetic Resonance in Medicine. Stockholm; 2010. p. 1641.

[10] Qin W, Yu CS, Zhang F, Du XY, Yan YX, Li KC. Effects of echo time on diffusion quantification of brain white matter at 1.5 T and 3.0 T. Magn Reson Med 2009;61:755–60.

[11] Huisman TAGM, Loenneker T, Barta G, Bellemann ME, Hennig J, Fischer JE, et al. Quantitative diffusion tensor MR imaging of the brain: field strength related variance of apparent diffusion coefficient (ADC) and fractional anisotropy (FA) scalars. Eur Radiol 2006;16: 1651–8.

[12] Jones DK, Horsfield MA, Simmons A. Optimal strategies for measuring diffusion in anisotropic systems by magnetic resonance imaging. Magn Reson Med 1999;42:515–25.

[13] Jones DK. The effect of gradient sampling schemes on measures derived from diffusion tensor MRI: a Monte Carlo study. Magn Reson Med 2004;51:807–15.

[14] Alexander AL, Hasan KM, Lazar M, Tsuruda JS, Parker DL. Analysis of partial volume effects in diffusion-tensor MRI. Magn Reson Med 2001;45:770–80.

[15] Pfefferbaum A, Sullivan EV. Increased brain white matter diffusivity in normal adult aging: relationship to anisotropy and partial voluming. Magn Reson Med 2003;49:953–61.

[16] Vos SB, Jones DK, Viergever MA, Leeman A. Partial volume effects as a hidden covariate in tractography based analysis of fractional anisotropy: does size matter? Proceedings of the Eighteenth Annual Meeting of the International Society of Magnetic Resonance in Medicine. Stockholm; 2010. p. 113.

[17] Oouchi H, Yamada K, Sakai K, Kizu O, Kubota T, Ito H, et al. Diffusion anisotropy measurement of brain white matter is affected by voxel size: underestimation occurs in areas with crossing fibers. Am J Neuroradiol 2007;28:1102–6.

[18] Landman BA, Farrell JAD, Huang H, Prince JL, Mori S. Diffusion tensor imaging at low SNR: nonmonotonic behaviors of tensor contrasts. Magn Reson Imaging 2008;26:790–800.

[19] Landman BA, Farrell JAD, Jones CK, Smith SA, Prince JL, Mori S. Effects of diffusion weighting schemes on the reproducibility of DTI-derived fractional anisotropy, mean diffusivity, and principal eigenvector measurements at 1.5T. NeuroImage 2007;36:1123–38.

[20] Kristoffersen A. Diffusion measurements and diffusion tensor imaging with noisy magnitude data. J Magn Reson Imaging 2009;29:237–41.

[21] Koay CG, Chang LC, Carew JD, Pierpaoli C, Basser PJ. A unifying theoretical and algorithmic framework for least squared methods of estimation in diffusion tensor imaging. J Magn Reson 2006;182: 115–25.

[22] Koay CG, Basser PJ. Analytically exact correction scheme for signal extraction from noisy MR signals. J Magn Reson 2006;179:317–22.

[23] Van Wedeen J, Hagmann P, Tseng WYI, Reese TG, Weisskoff RM. Mapping complex tissue architecture with diffusion spectrum magnetic resonance imaging. Magn Reson Med 2005;54:1377–86.

[24] Jensen JH, Helpern JA, Ramani A, Lu H, Kaczynski K. Diffusional kurtosis imaging: the quantification of non-Gaussian water diffusion by means of magnetic resonance imaging. Magn Reson Med 2005;53: 1432–40.

[25] Sammet S, Koch R, Irfanoglu OM, Schmalbrock P, Machiraju R, Knopp M. SENSE factor optimization for diffusion tensor imaging of the human brain at 7T. Proceedings of the Fifteenth Annual Meeting of the International Society of Magnetic Resonance in Medicine. Berlin; 2007.

[26] Morgan PS, Coxon RJ, Habib J, Gowland PA, Bowtell R. Comparison of sequences for improved diffusion weighted imaging at 7T. Proceedings of the Seventeenth Annual Meeting of the International Society of Magnetic Resonance in Medicine. Honolulu; 2009. p. 1807.

[27] Jaermann T, Pruessmann KP, Valavanis A, Kollias S, Boesiger P. Influence of SENSE on image properties in high-resolution single-shot echo-planar DTI. Magn Reson Med 2006;55:335–42.

[28] Alexander AL Lee JE, Wu YC, Field AS. Comparison of diffusion tensor imaging measurements at 3.0T versus 1.5T with and without parallel imaging. Neuroimaging Clin N Am 2006.

[29] Metcalf M, Pelletier D, Xu D, Okuda DT, Srinivasan R, Kelley D, et al. Diffusion tensor imaging at 7T: initial applications to multiple sclerosis. Proceedings of the Fifteenth Annual Meeting of the International Society for Magnetic Resonance in Medicine. Berlin; 2007. p. 2180.

[30] Dhital B, Turner R. Diffusion weighted imaging at 7T with STEAM-EPI and GRAPPA. Proceedings of the Eighteenth Annual Meeting of the International Society of Magnetic Resonance in Medicine. Stockholm; 2010. p. 3994.

[31] Mukherjee P, Hess CP, Xu D, Han ET, Kelley DA, Vigneron DB. Development and initial evaluation of 7-T *q*-ball imaging of the human brain. Magn Reson Imaging 2008;26:171–80.

[32] Heidermann RM, Porter DA, Anwander A, Feiweier T, Heberlein K, Knoesche TR, et al. Diffusion imaging in humans at 7T using readout segmented EPI and GRAPPA. Magn Reson Med 2010;64:9–14.

[33] Bernstein MA, King KF, Zhou ZJ. Handbook of MRI pulse sequences. Elsevier Academic Press: Burlington, MA; 2004. p. 620–4.

[34] Yarnykh VL. Actual flip-angle imaging in the pulsed steady state: a method for rapid three-dimensional mapping of the transmitted radiofrequency field. Magn Reson Med 2007;57:192–200.

[35] Preussmann KP, Weiger M Scheidergger MB, Boesinger P. SENSE: sensitivity encoding for Fast MRI. Magn reson Med 1999;42:952–62.

[36] Jiang H, van Zijl PCM, Kim J, Pearlson GD, Mori S. DtiStudio: resource program for diffusion tensor computation and fiber bundle tracking. Comput Methods Programs Biomed 2006;81:106–16.

[37] Taoka T, Iwasaki S, Sakamoto M, Nakagawa H, Fukusumi A, Myochin K, et al. Diffusion anisotropy and diffusivity of white matter tracts within the temporal stem in Alzheimer disease: evaluation of the "tract of interest" by diffusion tensor tractography. Am J Neuroradiol 2006;27:1040–5.

[38] Mihai G. Methods for brain iron evaluation in normal aging: T2 and phase measurements at 3 Tesla and 7 Tesla. Ph. D. Thesis, The Ohio State University, 2007.
[39] Pierpaoli C, Jezzard P, Basser PJ, Barnett A DiChiro G. Diffusion tensor imaging in the human brain. Radiology 1996;201:637–48.
[40] Piatkowski J, Storkey AJ, Bastin ME. Discovering white matter structure beyond fractional anisotropy maps. Proceedings of the Eighteenth Annual Meeting of the International Society of Magnetic Resonance in Medicine. Stockholm; 2010. p. 1574.
[41] Tsao S, Hwang DH, Singh M. CSF contamination correction in DTI tractography of the fornix in elderly subjects. Proceedings of the Eighteenth Annual Meeting of the International Society of Magnetic Resonance in Medicine. Stockholm; 2010. p. 1647.
[42] Kumazawa S, Yoshiura T, Honda H, Toyofuku F, Higashida Y. Development of partial volume segmentation of brain tissue based on diffusion tensor imaging (DTI). Proceedings of the Eighteenth Annual Meeting of the International Society of Magnetic Resonance in Medicine. Stockholm; 2010. p. 3126.
[43] Choi S, Cunningham D, Aguila F, Corrigan J, Bogner J, Mysiw WJ, et al. Systematic comparison of DTI at 7T and at 3T: assessment for FA for different acquisition protocols and SNR in healthy subjects. Proceedings of the Eighteenth Annual Meeting of the International Society of Magnetic Resonance in Medicine. Stockholm; 2010. p. 1602.
[44] Ibrahim TS, Mitchell C, Schmalbrock P, Lee R, Chakeres DW. Electromagnetic perspective on the operation of RF coils at 1.5-11.7 Tesla. Magn Reson Med 2005;54:683–90.
[45] Brunner DO, De Zanche N, Froehlich J, Paska J, Pruessmann KP. Traveling-wave nuclear magnetic resonance. Nature 2009;457:994–9.
[46] Sarlis JE, Luh WM, Pierpaoli C. Robust fat suppression for high-resolution diffusion weighted imaging. Proceedings of the Eighteenth Annual Meeting of the International Society of Magnetic Resonance in Medicine. Stockholm; 2010. p. 1612.
[47] Jeong HK, Anderson AW, Gore JC. Mufti-Shot SENSE DTI at 7T. Proceedings of the Eighteenth Annual Meeting of the International Society of Magnetic Resonance in Medicine. Stockholm; 2010. p. 1616.
[48] Pierpaoli C, Walker L, Irfanoglu MO, Barnett A, Basser P, Chang LC, et al. TORTOISE: an integrated software package for processing of diffusion MRI data. Proceedings of the Eighteenth Annual Meeting of the International Society of Magnetic Resonance in Medicine. Stockholm; 2010. p. 1616.
[49] Finsterbusch J. Fast-spin-echo imaging of inner fields-of-view with 2D-selective RF excitations. J Magn Reson Imaging 2010;31:1530–7.
[50] Von Morze J, Kelley DA, Banerjee S, Shephard TM, Xu D, Hess CP. Reduced field of view diffusion weighted imaging of the brain at 7T. Proceedings of the Eighteenth Annual Meeting of the International Society of Magnetic Resonance in Medicine. Stockholm; 2010. p. 3993.